On-Demand Nanodevice with Electrical and Neuromorphic Multifunction Realized by Local Ion Migration

Rui Yang,[†,*] Kazuya Terabe,[†,*] Guangqiang Liu,[†] Tohru Tsuruoka,[†] Tsuyoshi Hasegawa,[†] James K. Gimzewski,[†,‡,§] and Masakazu Aono[†]

[†]International Center for Materials Nanoarchitectonics (WPI-MANA), National Institute for Materials Science (NIMS), 1-1 Namiki, Tsukuba, Ibaraki 305-0044, Japan, [‡]Department of Chemistry and Biochemistry, University of California, Los Angeles, 607 Charles E. Young Drive East, Los Angeles, California 90095, United States, and [§]California NanoSystems Institute (CNSI), University of California, Los Angeles, 570 Westwood Plaza, Los Angeles, California 90095, United States

ABSTRACT A potential route to extend Moore's law beyond the physical limits of existing materials and device architectures is to achieve nanotechnology breakthroughs in materials and device concepts. Here, we discuss an on-demand WO_{3-x}-based nanoionic device where electrical and neuromorphic multifunctions are realized through externally induced local migration of oxygen ions. The device is found to possess a wide range of time scales of memorization, resistance switching, and rectification varying from volatile to permanent in a single device, and these can furthermore be realizable in both two- or three-terminal systems. The gradually changing volatile and nonvolatile resistance states are experimentally demonstrated to mimic the human brain's forgetting process for short-term memory and long-term memory.We propose this nanoionic device with its on-demand electrical and neuromorphic multifunction has a unique paradigm shifting potential for the fabrication of configurable circuits, analog memories, digital—neural fused networks, and more in one device architecture.

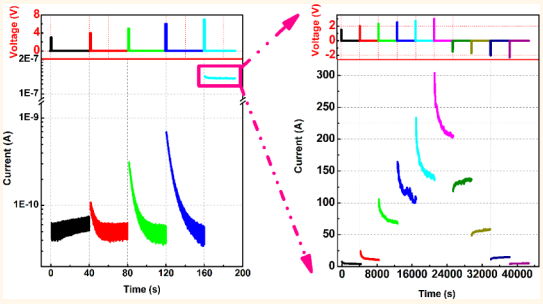

KEYWORDS: nanoionic device · resistance switching · memorization · rectification · neuromorphic properties

Conventional programmable circuits, such as field programmable gate arrays, enable users to locally change their functionality at any time to perform a multiplicity of functions, thereby offering advantages and flexibility for many technological applications.[1] However, this programmability comes at the expense of requiring massively parallel logic cells and switching cells to be constructed using traditional semiconductor nanodevices (predominantly transistors), resulting in large areas, low operation speeds, and high costs.[2] Additionally, the ultimate down-scaling of semiconductor transistors is already approaching its physical limits, and conventional Von Neumann architecture based on binary logic is becoming increasingly inefficient as the complexity of computation increases. This has promulgated the development of "next-generation" nanodevices that have unique functions and characteristics.[3] Devices with inherent synaptic function have recently been the subject of much interest and are considered to be essential building blocks in achieving artificial neural networks that attempt to emulate the highly efficient real-time capabilities of biological information processes.[4,5]

Detailed investigations into resistance switching phenomena[6−15] have recently revealed that artificial synaptic functions are a derivative phenomenon in resistance switching devices.[16−23] For instance, spike-time-dependent plasticity suggested by Hebbian learning has been observed in the devices with gradual nonvolatile resistance change by precisely controlling the parameters of the input electrical pulses.[17,20,21] An inherent learning ability was recently obtained in an Ag_2S-based atomic switch device,[18] which exhibited two conductance states: one in which the conductance rapidly faded away after weak signal inputs, analogous to short-term memory (STM), and another in which the conductance state was long-lived and stable, analogous to long-term memory (LTM). A transition between the two states could readily be achieved by

* Address correspondence to YANG.Rui@nims.go.jp; TERABE.Kazuya@nims.go.jp.

Received for review June 7, 2012 and accepted October 27, 2012.

Published online October 28, 2012
10.1021/nn302510e

controlling the input pulse repetition time. This atomic switch device, with its attractive synapse-like behaviors, required a nanogap structure, which is a technically challenging fabrication process. More recently, Chang *et al*. reported similar behaviors of STM and LTM transitions observed in a gapless Pd/WO_x/W device.[19] However, the "LTM" of their device persisted only for several minutes, implying that the device is capable of only volatile resistance switching without nonvolatile memory capacity.

A nanodevice that exhibits neuromorphic properties together with configurable digital/analog multifunctions will enable circuit fabrication using fewer elements with a smaller chip real estate. A requirement for this nanodevice is to possess a wide range of time scales of memorization varying from volatile to permanent. Here, we report experimental evidence that a single two-/three-terminal WO_{3-x}-based nanoionic device demonstrated nonvolatile/volatile bipolar resistance switching (BRS), rectification, and memory properties with controllable time scales by controlling the local migration of oxygen ions (described as oxygen vacancies, V_O). The device was switched from an insulated state to a temporal forward or reverse rectifier state depending on the polarity of the voltage pulses. The dependence of the gradually changing volatile and nonvolatile resistance states on time were then used to also mimic STM and LTM. The convergence of the configurable electronic and neuromorphic functions enabled this nanoionic device to work as an on-demand nanodevice with many potential applications.

RESULTS AND DISCUSSION

Present nanodevices have a simple stacked structure of Pt/WO_{3-x}/Pt. Configurable electrical and neuromorphic multifunctions are accomplised by controlling local oxygen migration at the Pt/WO_{3-x} interface. The V_O concentration has a strong effect on electrical conductivity in WO_{3-x} n-type semiconductors. The interface of Pt/WO_{3-x} exhibits ohmic characteristics with heavy V_O doping but exhibits rectification characteristics due to a Schottky-like barrier with light doping.[24] Since an V_O acts as a donor, the reduction of the V_O concentration at the Pt/WO_{3-x} interface will cause the depletion layer to become wider, resulting in an increase of the Schottky-like barrier at the Pt/WO_{3-x} interface and *vice versa*.[25] Our Pt/WO_{3-x}/Pt device that was in a pristine state demonstrated very high resistance values. The current−voltage curves ($I-V$) exhibited peculiar hysteresis characteristics when the applied voltage was swept between −2 and +2 V, as shown in Figure 1a. The resistance of the pristine device decreased nonlinearly after voltage sweeping in both positive and negative voltage regions. The states after voltage sweeping quickly decayed to the original state, as shown in the inset of Figure 1a, which means this resistance switching process is volatile. In contrast, after a positive or negative forming process, the device exhibited forward or reverse rectification and BRS properties (Figure 1b and c). The states obtained after voltage sweeping could be maintained for a long time in these cases, as shown in the insets of Figure 1b and c, which means BRS and rectification were nonvolatile. The positive (negative) forming process could be triggered by applying positive (negative) voltage sweeping or pulses on the top electrode to introduce a soft-breakdown with a current compliance of 0.5 mA; see Figure 1d.

It has been reported that the Ti adhesion layer penetrated the contact bottom Pt electrode with a thickness of 15 nm during the annealing process in a TiO_2-based device, and the bottom interface was turned to be an ohmic contact.[26] However, the Ti adhesion layer did not diffuse through the whole Pt bottom electrode with a thickness of 100 nm used in the present WO_{3-x}-based devices, which has been corroborated by the X-ray photoelectron spectroscopy (XPS) measurements. Moreover, the original $I-V$ curve of the device deposited on the bottom electrode with the Ti adhesion layer was almost the same as that of a device without a Ti adhesion layer. These results and the high initial resistance of the present device strongly suggest that Schottky-like barriers form at both the Pt TE/WO_{3-x} and WO_{3-x}/Pt BE interfaces, where TE indicates the top electrode and BE indicates that at the bottom, as shown in Figure 1d. During the forming process, conducting filaments with highly oxygen deficient $WO_{3-x-\delta}$ form similarly to the formation of the Magnéli phase (Ti_nO_{2n-1}) in TiO_{2-x}-based devices.[27] Applying a positive forming process apparently causes the Schottky-like barrier at the WO_{3-x}/Pt BE interface to collapse due to $V_O$formation and accumulation at the WO_{3-x}/Pt BE interface. However, the nonlinear $I-V$ curves (Figure 1b) indicate that the conducting channel does not entirely span the WO_{3-x} layer between TE and BE. Therefore, the remaining Schottky-like barrier at the Pt TE/WO_{3-x} interface generates rectification behavior, and modulation of this barrier results in BRS behavior. Since a residual Schottky-like barrier is located at either the TE or BE interface depending on the polarity of the forming voltage, this is consistent with the observed rectification and resistance switching behaviors with opposite polarities after negative forming process (Figure 1c).

In the pristine state, the current in the positive region instantaneously increased while the negative region displayed no distinct increase after application of a positive voltage pulse, resulting in the rectification characteristics shown in Figure 2a. Reverse rectification was readily achieved by the application of negative pulses. Such rectification behavior was observed only immediately after applying the pulses, which are not enough to trigger the forming process. The current subsequently faded quickly and returned to its original value within ~100 s after the pulse was applied; see Figure 2b. The X-ray photoelectron spectroscopy analysis indicated the WO_{3-x} film used in the present device had

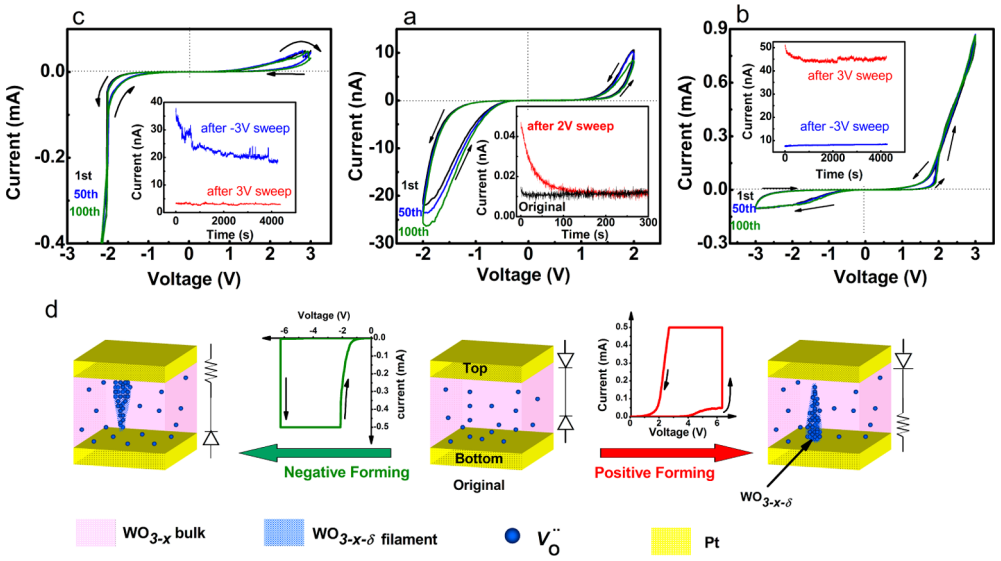

Figure 1. Electrical characterization of the Pt/WO_{3-x}/Pt devices before and after the forming process. *I*–*V* curves (1st, 50th, and 100th) of Pt/WO_{3-x}/Pt device in (a) pristine state, (b) after positive forming process, and (c) after negative forming process. Inset in panel a plots the retention characteristics of original state and that obtained after voltage sweeping to 2 V. Read voltage was 0.5 V. Insets in panels b and c plot the retention characteristics of high and low resistance states obtained after corresponding voltage sweeping. Read voltage was 0.1 V. (d) Schematic illustration and equivalent circuit of device before (middle) and after positive (right) and negative (left) forming process. Positive and negative forming processes are also shown.

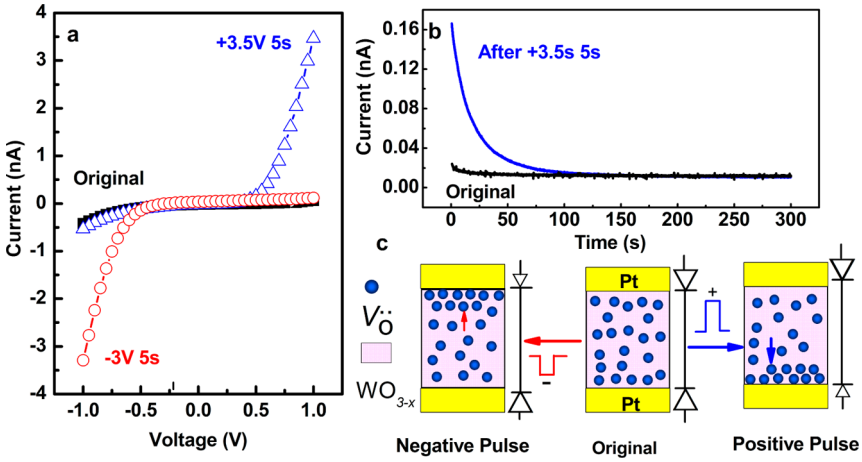

Figure 2. Configurable volatile rectification behavior observed in two-terminal devices. (a) *I*–*V* characteristics of two-terminal device in original state and after applying positive and negative electric pulses. (b) Current variation over time for original state and that immediately after positive voltage pulses were applied. Read voltage was 0.5 V. (c) Schematic illustrations of oxygen vacancy profiles and equivalent circuits when device was in original state and when positive and negative pulses were applied immediately after pulses.

a certain amount of V_O that formed during the preparation process (see Figure S1 in the Supporting Information). Hard X-ray photoelectron spectroscopy under bias operation measurements directly indicated that oxygen migration could occur at the Pt/WO_{3-x} interface under external bias. The V_O concentration at the Pt TE/WO_{3-x} interface decreased by applying positive bias and increased by applying negative bias (see Section 2 in the Supporting Information). Based on these results, a plausible mechanism for this reconfigurable volatile rectification is illustrated in Figure 2c. Here, the concentration of V_O at the Pt/WO_{3-x} interface could be electrically controlled by applying an external voltage pulse. When a positive pulse was applied to Pt TE, the external electrical field mainly dropped at the WO_{3-x}/Pt BE interface. The V_O migration and accumulation at the WO_{3-x}/Pt BE interface lowered the effective Schottky-like barrier. In contrast, the barrier slightly increased or at least remained unchanged in height at the Pt TE/WO_{3-x} interface. Therefore, the WO_{3-x}/Pt TE interface dominated the carrier transport process and exhibited forward rectification. The subsequent relaxing of the V_O that accumulated at the bottom interface due to the electrochemical potential gradient accounted well for the volatile characteristics of this

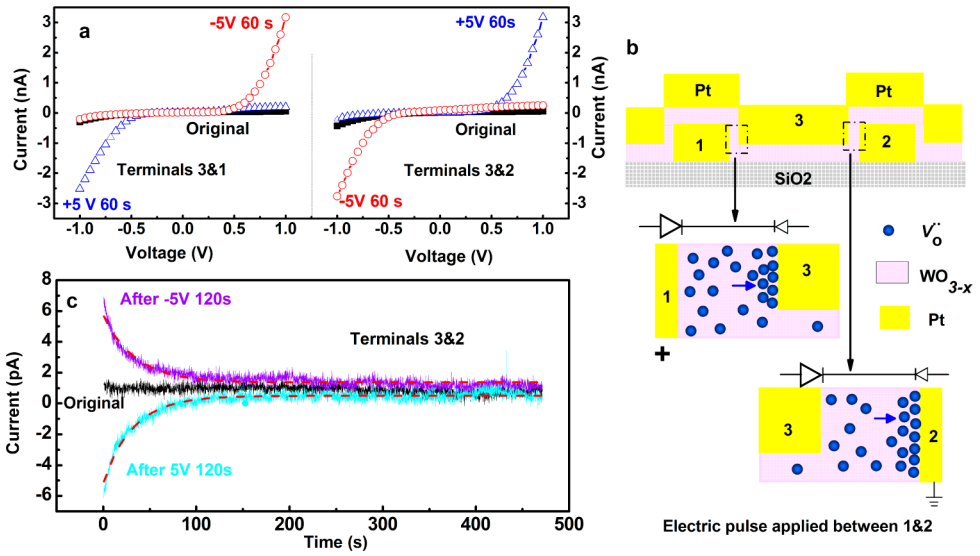

Figure 3. Configurable volatile rectification behavior observed in three-terminal devices. (a) *I*−*V* characteristics of three-terminal device in pristine state and after positive and negative electric pulses were applied between terminals 1 and 2. (b) Schematic illustrations of three-terminal device, oxygen vacancy profiles, and equivalent circuits for device immediately after positive pulses were applied between terminals 1 and 2. (c) Variations over time for current between terminals 3 and 2 for original state and immediately after positive and negative electric pulses were applied between terminals 1 and 2. Read voltage was not applied during measurements. Both current fade processes were well fitted by the exponential function $I = A \exp(Bt)$, where *I* is current, *t* is time, and *A* and *B* are fitting constants. Dashed lines are fitting curves.

rectification behavior. When a negative voltage pulse was applied to the Pt TE, the V_O locally migrated in the opposite direction, resulting in reverse rectification. Only devices having electrodes with high work functions, such as Pt and Au, exhibit this reproducible volatile rectification (Figure S3 in the Supporting Information), which is consistent with the proposed mechanism involving a Schottky-like barrier at the interface. We found that reconfigurable volatile rectification could also be achieved in an oxygen environment without moisture, indicating it is dominantly related to the local V_O migration rather than proton-induced effects. Moreover, the device showed distinct reverse rectification in vacuum or N_2 gas under no external electric field, and the device recovered to the original insulating state with no rectification when the environment was changed back to the air or O_2 gas (Supporting Information Figure S4). Since oxygen can easily diffuse along grain boundaries in a Pt electrode,[28] the V_O concentration at the Pt TE/WO_{3-x} interface could increase due to the oxygen evaporation through the Pt TE in a vacuum, resulting in lowering of the Schottky-like barrier in the top interface and then the appearance of the reverse rectification under vacuum. These results also indicated that the reconfigurable volatile rectification behavior was related to the local oxygen migration at the Pt/WO_{3-x} interface.

In the three-terminal device, volatile rectification could also be achieved by applying voltage pulses to one terminal and measuring the current between the other terminals. As shown in Figure 3a, after a voltage pulse was applied between terminals 1 and 2, the *I*−*V* curve measured between terminals 3 and 2 exhibited rectification. Moreover, the *I*−*V* curve measured between terminals 3 and 1 showed rectification with opposite polarity. This behavior is consistent with local V_O migration in the interface regions, resulting in volatile rectification (Figure 3b). Note that our three-terminal device was electronically equivalent to two volatile forward and reverse two-terminal rectifying devices in parallel. From Figure 3c, we can see that the current between terminals 3 and 2 faded exponentially with time after positive and negative voltage pulses were applied between terminals 1 and 2.

The current fading process after a sequence of input pulses in the two-terminal device was systemically investigated. As shown in Figure 4a, instantaneous current was observed to increase gradually as the amplitude of applied voltage pulses was increased. This current was then observed to decay back to the original state. However, after a high-voltage pulse (7 V) was applied to initiate the forming process, the current persisted in a high-level state, and the device exhibits unique BRS characteristics, as shown in Figure 4b. First, multiple resistance states were observed by applying voltage pulses with different amplitudes. Second, the high current achieved through inputting positive voltage pulses automatically faded over time but did not return to the original state even over a measurement period of 24 h after pulse application, which indicates partial memorization. Third, the intermediate state, obtained by applying negative voltage pulses, was stable and no temporal fading in the current was observed, as shown in Figure 4c. These phenomena originate from the unique oxygen migration process involved in BRS behavior, which has been systematically studied through investigations into the effect

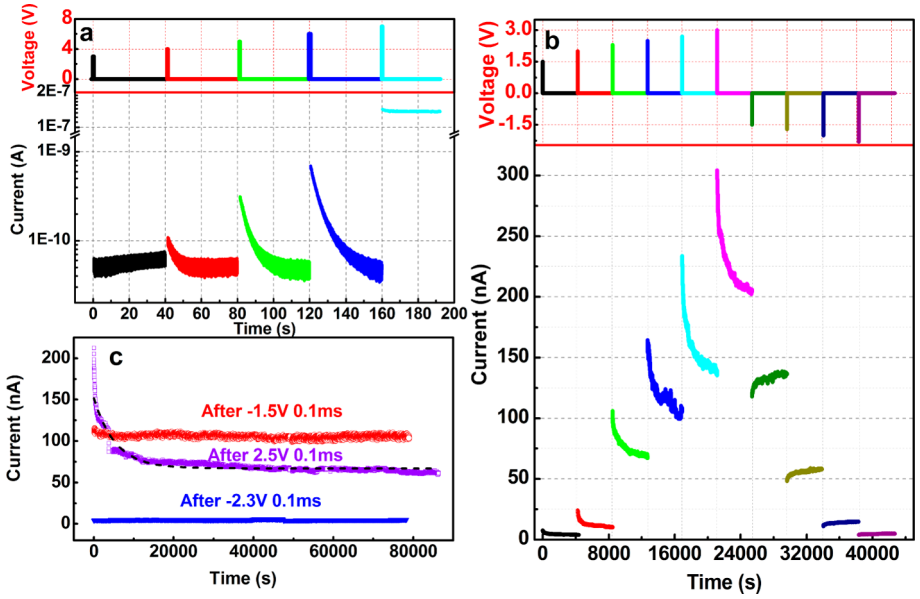

Figure 4. Volatile and nonvolatile memory properties of Pt/WO_{3-x}/Pt device. (a) Current change observed in two-terminal device by applying sequence of positive voltage pulses at intervals of 40 s and widths of 0.5 s. Read voltage was 0.5 V. (b) Current change observed in two-terminal device after forming process following application of sequence of positive and negative pulses with widths of 0.1 ms. Read voltage was 0.1 V. (c) Retention characteristics of three states after application of electric pulse: 2.5 V/0.1 ms, −1.5 V/0.1 ms, and −2.3 V/0.1 ms. Current fade processes after application of 2.5 V/0.1 ms pulse are well fitted by exponential function indicated by dashed line.

of the atmosphere and electrode materials on BRS behavior in WO_{3-x}-based nanoionics device.[29] It was found that the oxygen migration process during BRS behavior mainly occurred between the Pt/WO_{3-x} interface and Pt electrode. The high catalytic activity and oxygen absorbability of the Pt electrode are indispensable for realizing stable BRS behavior at the Pt/WO_{3-x} interface.[28,30] Oxygen migrates from the Pt TE into the Pt TE/WO_{3-x} interface under a negative electrical field with a reduction reaction of $1/2\ O_{2(in\ \ Pt)} + 2e' + V_O \rightarrow O_o^x$, resulting in the annihilation of V_O in the interface region and resistance increase ($O_{2(in\ \ Pt)}$ and O_o^x indicate the absorbed oxygen in Pt TE and the oxygen in WO_{3-x}, respectively). The opposite process occurs under a positive electric field with a reaction of $O_o^x \rightarrow 1/2\ O_{2(in\ \ Pt)} + 2e' + V_O$, as has been proposed for NiO-[31] and $SrTiO_3$[32]-based devices. The electrical Joule heating effect may enhance the oxygen migration and redox reaction at the interface in the resistance switching process. The current decay observed after application of a positive voltage pulse is attributed to oxygen diffusion occurring relatively easily from the Pt TE into the interface region due to the electrochemical potential gradient between the Pt electrode and the interface region. In contrast, the oxygen ions that migrate into the interface region under a negative electric field may be relatively stable because the diffusion back from the interface region to the Pt TE with the generation of oxygen gas does not easily occur. Therefore, states obtained by applying negative pulses are much more stable than those obtained by applying positive ones. The three-terminal devices exhibited similar volatile and nonvolatile memorization (Figure S5 in the Supporting Information).

The wide range of time scales for memorization varying from volatile to permanent realized in the present device is suitable for imitating the equivalent of the Ebbinghaus forgetting process.[33] Before the forming process is applied, the memorization is volatile, which is analogous to STM in the human brain (the source of memory created by weak stimulation is exponentially forgotten until none remains).[18] After the forming process is applied, partial and complete nonvolatile memorization can be obtained by controlling the polarity of the input pulse. Interestingly, the current fading process, after application of the positive voltage pulse, fits the exponential function well, which is analogous to the Ebbinghaus forgetting curve,[33] where some but not all the memory source is forgotten over time. The forgotten part is ascribed to STM, and the memorized part is clearly LTM, which exponentially fades over time but with a longer time constant. Moreover, the savings score can be gradually increased, step-by-step, by reinforcing the input stimulus. This can be imitated in the present device by gradually increasing the amplitude of the voltage pulse, as shown in Figure 4b. The LTM can then be erased step-by-step by applying negative pulses. These data indicate that a "multistore model" of human memory[34] can also be implemented in the present nanodevice (see Section 6 in the Supporting Information). Note that the current observed in volatile memorization is much lower than that in partial nonvolatile memorization in the present WO_{3-x}-base nanodevice. The current of the nonvolatile

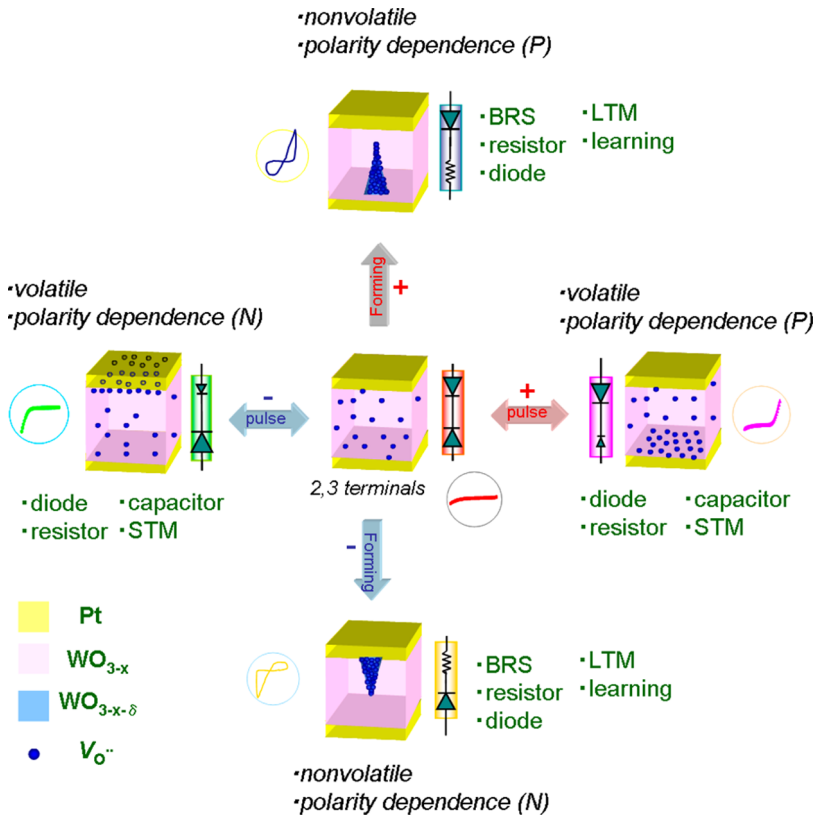

Figure 5. Schematic depiction of the configurable electric and neuromorphic multifunctions realized in the WO_{3-x}-based devices. *P* and *N* indicate the dependence of positive and negative polarity on the external field of volatile and nonvolatile electric and neuromorphic multifunctions, respectively.

memorization can be decreased to the comparable value with that of the volatile memorization by decreasing the current compliance in the forming process and the amplitude of the applied pulses (see Section 7 in the Supporting Information).

SUMMARY AND CONCLUSIONS

We demonstrated an on-demand nanodevice with configurable electronic and neuromorphic functions in a two-/three-terminal WO_{3-x}-based device with a simple stacked structure (see Figure 5). Multifunctional properties including volatile and nonvolatile rectifications as well as bipolar resistance switching behaviors were attainted in one device by just controlling the local migration of oxygen ions. The achievement of memorization with a wide range of time scales enabled the "forgetting process" observed in biological information processing to be imitated. Even though the nonvolatile memorization needs an irreversible forming process, the as-prepared nanodevice was controllably preprogrammed to perform a large variety of functions at will and is shown to be used as a variable resistance element, a diode, a switch, or a neuromorphic memory. These capabilities open a new avenue for circuits, analog memories, and artificially fused digital–neural networks using programming by input pulse polarity, magnitude, and repetition history.

EXPERIMENTAL SECTION

A thin WO_{3-x} film with a thickness of 60 nm was prepared by radio frequency sputtering on a Pt bottom electrode with a quartz glass substrate at room temperature. The deposition was performed starting with a polycrystalline WO_3 target in a gas mixture containing 80% Ar and 20% O_2 at a pressure of 0.93 Pa. The WO_{3-x} layer was then annealed *in situ* at 300 °C in an oxidizing atmosphere containing 50% Ar and 50% O_2 at a pressure of 2.67 Pa. Both the Pt TE and BE electrodes were 100 nm thick and were deposited in a pure Ar environment using a metal mask. The three-terminal device was fabricated by simultaneously depositing two bottom Pt electrodes, 0.2 mm apart, on a quartz glass substrate using a metal mask. Each two-terminal device consisted of a cross-point structure with a junction area of 25 × 25 μm. The three-terminal device consisted of two cross-point structures, as shown in Figure 3b. The element chemical state of the WO_{3-x} film was analyzed using X-ray photoelectron spectroscopy (Thermo Scientific, Theta Probe) with monochromatic Al Kα X-rays (beam-spot diameter = 400 μm). The Pt (6 nm)/WO_{3-x} interface electronic states under external electrical bias were measured using hard X-ray photoelectron spectroscopy in the Spring 8 BL15XU undulator beamline. The dc *I*–*V* curves were measured using a high-vacuum four-probe system equipped with a semiconductor characterization system (Keithley 4200SCS). All measurements were performed at room temperature. For the two-terminal device, the bottom electrode was grounded, and an electric field was applied to the top electrode. For the three-terminal devices, voltage pulses were applied to terminal 1, while terminal 2 was grounded and terminal 3 was floating. The *I*–*V* curves between

terminals 3 and 2 were then immediately measured, while terminal 1 was floating. During the measurement, voltage was applied to terminal 3 and terminal 2 was grounded, as was done in measuring the two-terminal device. The $I-V$ characteristics between terminals 3 and 1 were also measured in this way.

Conflict of Interest: The authors declare no competing financial interest.

Supporting Information Available: Electrical conductivity and XPS analysis of WO_{3-x} films deposited under different gas mixtures; hard X-ray photoelectron spectroscopy under bias operation measurements at the Pt (6 nm)/WO_{3-x} interface; effect of electrode materials and environment on the electrical properties of the *Metal*/WO_{3-x}/Pt devices (*Metal* = Pt, Au, Ag, Cu, W, Ti, and Al); volatile and nonvolatile memory properties observed in three-terminal devices; "multistore model" of human memory implemented in the present device; reducing the current gap between volatile memorization and nonvolatile memorization. This material is available free of charge *via* the Internet at http://pubs.acs.org.

Acknowledgment. We thank T. Ohno of National Institute for Materials Science (NIMS) for the fruitful discussion about the neuromorphic property, and H. Yoshikawa and T. Tsuchiya of NIMS for their help with hard X-ray photoelectron spectroscopy measurements.

REFERENCES AND NOTES

1. Rose, J.; Elgamal, A.; Sangiovanni-Vincentelli, A. Architecture of Field-Programmable Gate Arrays. *Proc. IEEE* **1993**, *81*, 1013–1029.
2. Kaeriyama, S.; Sakamoto, T.; Sunamura, H.; Mizuno, M.; Kawaura, H.; Hasegawa, T.; Terabe, K.; Nakayama, T.; Aono, M. A Nonvolatile Programmable Solid-Electrolyte Nanometer Switch. *IEEE J. Solid-State Circuit* **2005**, *40*, 168–176.
3. Vogel, E. M. Technology and Metrology of New Electronic Materials and Devices. *Nat. Nanotechnol.* **2007**, *2*, 25–32.
4. Strukov, D. B. Nanotechnology Smart Connections. *Nature* **2011**, *476*, 403–405.
5. Wijekoon, J. H. B.; Dudek, P. Compact Silicon Neuron Circuit with Spiking and Bursting Behaviour. *Neural Networks* **2008**, *21*, 524–534.
6. Liu, S. Q.; Wu, N. J.; Ignatiev, A. Electric-Pulse-Induced Reversible Resistance Change Effect in Magnetoresistive Films. *Appl. Phys. Lett.* **2000**, *76*, 2749–2751.
7. Waser, R.; Aono, M. Nanoionics-Based Resistive Switching Memories. *Nat. Mater.* **2007**, *6*, 833–840.
8. Yao, J.; Sun, Z. Z.; Zhong, L.; Natelson, D.; Tour, J. M. Resistive Switches and Memories From Silicon Oxide. *Nano Lett.* **2010**, *10*, 4105–4110.
9. Waser, R.; Dittmann, R.; Staikov, G.; Szot, K. Redox-Based Resistive Switching Memories - Nanoionic Mechanisms, Prospects, and Challenges. *Adv. Mater.* **2009**, *21*, 2632–2663.
10. Kozicki, M. N.; Gopalan, C.; Balakrishnan, M.; Mitkova, M. A Low-Power Nonvolatile Switching Element Based on Copper-Tungsten Oxide Solid Electrolyte. *IEEE Trans. Nanotechnol.* **2006**, *5*, 535–544.
11. Xu, Z.; Bando, Y.; Wang, W. L.; Bai, X. D.; Golberg, D. Real-Time *in Situ* HRTEM-Resolved Resistance Switching of Ag_2S Nanoscale Ionic Conductor. *ACS Nano* **2010**, *4*, 2515–2522.
12. Nagashima, K.; Yanagida, T.; Oka, K.; Taniguchi, M.; Kawai, T.; Kim, J. S.; Park, B. H. Resistive Switching Multistate Nonvolatile Memory Effects in a Single Cobalt Oxide Nanowire. *Nano Lett.* **2010**, *10*, 1359–1363.
13. He, C. L.; Shi, Z. W.; Zhang, L. C.; Yang, W.; Yang., R.; Shi, D. X.; Zhang, G. Y. Multilevel Resistive Switching in Planar Graphene/SiO_2 Nanogap Structures. *ACS Nano* **2012**, *6*, 4214–4221.
14. Tsuchiya, T.; Oyama, Y.; Miyoshi, S.; Yamaguchi, S. Nonstoichiometry-Induced Carrier Modification in Gapless Type Atomic Switch Device Using Cu_2S Mixed Conductor. *Appl. Phys. Express* **2009**, *2*, 055002.
15. Liu, Q.; Sun, J.; Lv, H. B.; Long, S. B.; Yin, K. B.; Wan, N.; Li, Y. T.; Sun, L. T.; Liu, M. Real-Time Observation on Dynamic Growth/Dissolution of Conductive Filaments in Oxide-Electrolyte-Based ReRAM. *Adv. Mater.* **2012**, *24*, 1844–1849.
16. Krzysteczko, P.; Munchenberger, J.; Schafers, M.; Reiss, G.; Thomas, A. The Memristive Magnetic Tunnel Junction as a Nanoscopic Synapse-Neuron System. *Adv. Mater.* **2012**, *24*, 762–766.
17. Kuzum, D.; Jeyasingh, R. G. D.; Lee, B.; Wong, H.-S. P. Nanoelectronic Programmable Synapses Based on Phase Change Materials for Brain-Inspired Computing. *Nano Lett.* **2012**, *12*, 2179–2186.
18. Ohno, T.; Hasegawa, T.; Tsuruoka, T.; Terabe, K.; Gimzewski, J. K.; Aono, M. Short-Term Plasticity and Long-Term Potentiation Mimicked in Single Inorganic Synapses. *Nat. Mater.* **2011**, *10*, 591–595.
19. Chang, T.; Jo, S.-H.; Lu, W. Short-Term Memory to Long-Term Memory Transition in a Nanoscale Memristor. *ACS Nano* **2011**, *5*, 7669–7676.
20. Jo, S. H.; Chang, T.; Ebong, I.; Bhadviya, B. B.; Mazumder, P.; Lu, W. Nanoscale Memristor Device As Synapse in Neuromorphic Systems. *Nano Lett.* **2010**, *10*, 1297–1301.
21. Yu, S. M.; Wu, Y.; Jeyasingh, R.; Kuzum, D. G.; Wong, H. S. P. An Electronic Synapse Device Based on Metal Oxide Resistive Switching Memory for Neuromorphic Computation. *IEEE Trans. Electron Devices* **2011**, *58*, 2729–2737.
22. Alibart, F.; Pleutin, S.; Bichler, O.; Gamrat, C.; Serrano-Gotarredona, T.; Linares-Barranco, B.; Vuillaume, D. A Memristive Nanoparticle/Organic Hybrid Synapstor for Neuroinspired Computing. *Adv. Funct. Mater.* **2012**, *22*, 609–616.
23. Wang, Z. Q.; Xu, H. Y.; Li, X. H.; Yu, H.; Liu, Y. C.; Zhu, X. J. Synaptic Learning and Memory Functions Achieved Using Oxygen Ion Migration/Diffusion in an Amorphous InGaZnO Memristor. *Adv. Funct. Mater.* **2012**, 10.1002/adfm.201103148.
24. Yang, J. J.; Borghetti, J.; Murphy, D.; Stewart, D. R.; Williams, R. S. A Family of Electronically Reconfiguiable Nanodevices. *Adv. Mater.* **2009**, *21*, 3754–3758.
25. Sawa, A. Resistive Switching in Transition Metal Oxides. *Mater. Today* **2008**, *11*, 28–36.
26. Yang, J. J.; Strachan, J. P.; Xia, Q. F.; Ohlberg, D. A. A.; Kuekes, P. J.; Kelley, R. D.; Stickle, W. F.; Stewart, D. R.; Medeiros-Ribeiro, G.; Williams, R. S. Diffusion of Adhesion Layer Metals Controls Nanoscale Memristive Switching. *Adv. Mater.* **2010**, *22*, 4034–4038.
27. Kwon, D. H.; Kim, K. M.; Jang, J. H.; Jeon, J. M.; Lee, M. H.; Kim, G. H.; Li, X. S.; Park, G. S.; Lee, B.; Han, S.; *et al*. Atomic Structure of Conducting Nanofilaments in TiO_2 Resistive Switching Memory. *Nat. Nanotechnol.* **2010**, *5*, 148–153.
28. Schmiedl, R.; Demuth, V.; Lahnor, P.; Godehardt, H.; Bodschwinna, Y.; Harder, C.; Hammer, L.; Strunk, H. P.; Schulz, M.; Heinz, K. Oxygen Diffusion Through Thin Pt Films on Si(100). *Appl. Phys. A-Mater. Sci. Process* **1996**, *62*, 223–230.
29. Yang, R.; Terabe, K.; Tsuruoka, T.; Hasegawa, T.; Aono, M. Oxygen Migration Process in The Interfaces During Bipolar Resistance Switching Behavior of WO_{3-x}-based Nanoionics Devices. *Appl. Phys. Lett.* **2012**, *100*, 231603.
30. Galvagno, S.; Parravano, G. Supported Au-Pt Catalysts Characterization And Hydrogen Transfer Activity Between Benzene And Cyclohexane. *J. Catal.* **1979**, *57*, 272–286.
31. Yoshida, C.; Kinoshita, K.; Yamasaki, T.; Sugiyama, Y. Direct Observation of Oxygen Movement During Resistance Switching in NiO/Pt Film. *Appl. Phys. Lett.* **2008**, *93*, 042106.
32. Jeon, S. H.; Park, B. H.; Lee, J.; Lee, B.; Han, S. First-Principles Modeling of Resistance Switching in Perovskite Oxide Material. *Appl. Phys. Lett.* **2006**, *89*, 042904.
33. Ebbinghaus, H. In *Memory: A Contribution to Experimental Psychology*; Ruger, H. A.; Bussenius, C. E., Eds. trans.; Teachers College: Columbia University, 1913.
34. Atkinson, R. C.; Shiffrin, R. M. In *The Psychology of Learning and Motivation: Advances in Research and Theory*; Spence, K. W.; Spence, J. T., Eds.; Academic: New York, 1968; pp 89–195.